

Phase and Lyot-type coronagraphs for the High Order Testbench: prototyping and first laboratory results

Patrice Martinez^{*a, b, e}, Elise Vernet^a, Christophe Dorrer^c, Emmanuel Aller Carpentier^a, Anthony Boccaletti^{b, e}, Markus Kasper^a, Jacques Baudrand^{b, e}, Christine Chaumont^{d, e}

^a European Southern Observatory, Adaptive optics Department – Telescope System Division - Karl Schwarzschild Str. 2 - D-85748 Garching Bei München - Germany

^b Observatoire de Paris Meudon (LESIA), 5 place Jules Janssen, 92190 Meudon, France

^c Laboratory for Laser Energetics-University of Rochester, 250 East River Rd, Rochester, NY, 14623-USA

^d Observatoire de Paris Meudon (GEPI), 5 place Jules Janssen, 92190 Meudon, France

^e Groupement d'intérêt scientifique PHASE (Partenariat Haute résolution Angulaire Sol Espace)

ABSTRACT

We report laboratory development of coronagraphic devices to be implemented on the High Order Testbench (HOT) to assess intensity reduction between them at a high Strehl ratio regime. The high order test bench implements extreme adaptive optics with realistic telescope conditions reproduced by star and turbulence generators. A 32×32 actuator micro deformable mirror, one pyramid wave front sensor, one Shack-Hartmann wave front sensor and the ESO SPARTA real-time computer. This will enable characterization and comparative study of different types of coronagraphs in realistic conditions. We have developed several prototypes of promising coronagraphs concepts: Four Quadrants Phase Mask¹ (FQPM), Lyot² coronagraphs and Apodized Pupil Lyot Coronagraph³ (APLC). We will describe the design of the IR coronagraphic path on HOT, prototyping processes used for each coronagraph and discuss quality control and first results obtained on a IR coronagraphic testbench (Strehl ratio ~ 94%). Finally, we will present our experiment plan and future coronagraph developments.

Keywords : high angular resolution, Extreme adaptive optics, coronagraphy

INTRODUCTION

A coronagraph used in conjunction with AO system can improve the sensitivity of an imaging system to faint structure surrounding a bright source. These devices block the core of the image of an on-axis source and suppress the bright diffraction rings and halo, removing light that would otherwise reduce the dynamic range of the imaging. This enables faint off-axis objects to be observed. The state-of-the-art of coronagraphy has impressively evolved during the last ten years. Coronagraphs are now able to provide a very large on-axis extinction as demonstrated in laboratory conditions. But their capabilities during sky observations are damped by the large amount of residual phase aberrations that are left uncorrected by the AO system. Coronagraphy is a mandatory technique to suppress on-axis starlight, but a coronagraph can only reduce the contribution of the coherent part of the light. Hence, their capabilities on sky are in strong relation with AO efficiencies.

Any high contrast instrument concepts for large ground-based telescopes such as SPHERE⁴, GPI⁵ or EPICS⁶ for the future E-ELT use a combination of XAO and a coronagraph.

Therefore, implementation of coronagraphs on HOT provide an ideal environment to assess the contrast delivered by each device considering the diffraction by the edges of the pupil and the residual phase aberrations that are leaking through the AO system. We have produced several coronagraphs to compare them in this advantageous environment. Hopefully, outputs of this comparison will present the possibility to extend this study to the case of Extremely Large Telescopes.

* martinez@eso.org, phone: +498932006398

1. OPTICAL SETUP OVERVIEW

The High Order Testbench (HOT, see Fig. 1) implements an XAO system on the MACAO (Multi Application Curvature Adaptive Optics) test bench which includes star and turbulence generators to mimic realistic conditions at a telescope. The bench is installed at ESO/Garching. Responsibilities are split between ESO (DM, the optical setup, and the SHWS RTC), Durham University (SHS) and Arcetri (PWS including its dedicated RTC). In this section we will further discuss the IR coronagraphic optical path of HOT, more details on AO common path optics, optical quality, turbulence generator and phase screens, micro deformable mirror, SHWS, PWS and laboratory demonstration are presented in separate papers^{7,8}.

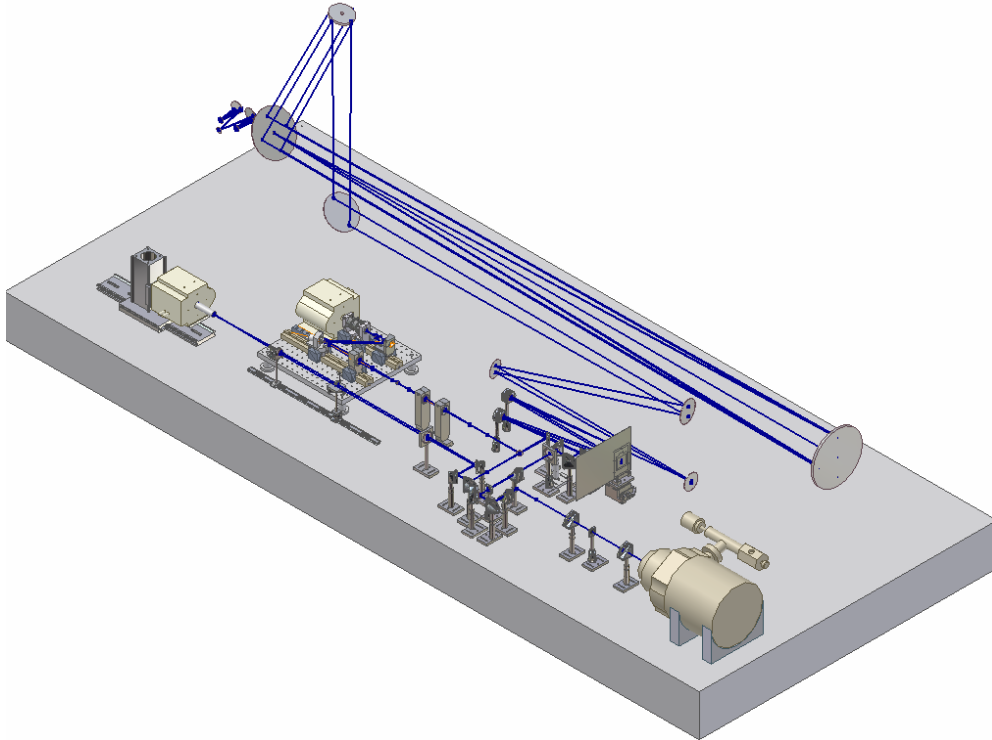


Figure 1 : Schematic HOT setup on the MACAO testbench including IR coronagraphic path

To avoid any delay in the AO implementation/work on HOT, the IR coronagraphic path has been mounted and installed on a separate bench. So, this separate IR coronagraphic test bench mimics the IR coronagraphic optical path of HOT. The optical system was designed using the optics program ZEMAX. The optical setup is designed to simulate the 8 m VLT pupil. It does so by scaling the 8 m VLT pupil to $3\text{ mm} \pm 0.002\text{ mm}$ using a laser-cut stainless steel sheet. The central obscuration is scaled to $0.47\text{ mm} \pm 0.002\text{ mm}$. The spider vanes thickness has an incorrect value ($60\text{ }\mu\text{m}$ instead of $15\text{ }\mu\text{m}$) in our first pupil mask. This will somehow impact coronagraphic tests since most of the time pupil stops have oversized spider vanes to get rid of misalignment problems (APLC) or to block light diffracted by the spider vanes of the pupil that is leaking through the coronagraph and reappears in the relayed pupil (FQPM, Lyot). Update of the pupil mask with 15-micron vanes has been ordered and is currently tested.

The test bench uses an F/48.4 at the coronagraphic focal plane. Our coronagraphic system consists of $\lambda/10$ IR achromatic doublets. We use a broadband white-light source combined either with an IR narrow filter ($R = 70$, central wavelength of $1.64\text{ }\mu\text{m}$, $\text{BW} = 0.024\text{ nm}$ with a peak transmission of 64.4%, checked with an FTS) or multiple choice of IR filter, installed inside the IR camera and accessible through a filter wheel, in J, H, and K band. In practice, most of the time we use a broadband H filter (center at $1.6\text{ }\mu\text{m}$, $R = 5$) combined or not with the H narrow external one presented previously. The camera used is the ITC (Infrared Test Camera), cooled at 103 K degree with a vacuum of 10^{-5} mbar. The Strehl ratio was evaluated at 94%. It was determined by measuring the peak level of an experimental PSF divided by its total flux, divided by the peak level of a theoretical PSF divided by its total flux. The theoretical PSF is created by performing the

forward fast Fourier transform of the autocorrelation of an oversampled and uniformly illuminated entrance pupil image from our telescope pupil mask (Fig. 2, left). Our pupil and focal planes masks are mounted on (x, y, z, θ) stages to minimize positioning error.

2. CORONAGRAPH PROTOTYPING

Several coronagraph concepts have been developed in the frame of WP 04500 of ELT design study such as the Four Quadrant Phase Mask, non-apodized Lyot coronagraphs and the Apodized Pupil Lyot Coronagraph. In the following, we describe the main characteristics of these devices and manufacturing considerations as well.

2.1 Four Quadrants Phase Mask

As a baseline, the FQPM chosen for HOT are monochromatic. Achromatic devices (either FQPMs using half-waves plates¹⁰ or AGPM¹¹) will be implemented on HOT in the framework of EPICS phase A in the next future. FQPM was developed by GEPI (Galaxies Etoiles Physique et Instrumentation) from Paris Observatory.

Derived requirements of the mask – The manufactured FQPM must be as close to the theoretically perfect FQPM as possible to reach the expected performance. One can expect not to be limited by the intrinsic manufactured defects of the component. To do so, the manufactured FQPM as been specified to deliver performance that correspond to the case where the limitation only comes from the diffraction by the edges of the pupil (VLT-like pupil at the entrance pupil of HOT). In this ideal case, uncorrected aberrations that are leaking through the AO system are not considered but will decrease the FQPM efficiency when implemented on HOT. Accuracy of critical parameters that GEPI has reached are detailed hereafter and presented in Table 1 where we compare performance imposed by manufactured defects to ideal performance expected when the Strehl ratio is 100%. A microscope inspection of the quadrants is presented in Fig. 3. The total nulling of the coronagraph refers to the total rejection rate (τ): ratio of the total integrated intensity with and without the FQPM.

Operating wavelength precision – The monochromatic FQPM is manufactured by engraving of two opposite quadrants on an optical medium. The thickness of the FQPM step directly defines the optimal wavelength λ_0 for which the attenuation is the best. A difference between the optimized and the working wavelength λ reduces the attenuation of the FQPM¹². A dedicated visible spectroscopic bench was used at LESIA (Laboratoire d'Etudes Spatiales et d'Instrumentation en Astrophysique, from Paris Observatory) to measure the thickness of the FQPM step¹². A precision of less than 3% was required on the FQPM step thickness, GEPI has reached a depth accuracy of 0.2% (see Table 1).

FQPM transition precision – Ideally the transition between the four quadrants must be infinitely small. Departure from this ideal case decreases the capability of the real device¹². Microscopic inspection of the manufactured FQPM (Fig. 3, right) shows that the transition quality is less then 1 μm (2 μm peak-to-peak transitions). The impact of this defects is estimated in Table 1. At this level, the efficiency of the FQPM will be set by external parameters (diffraction of the pupil).

Chromaticity – The chosen FQPM is monochromatic. The effect of chromaticity has been defined in previous paper¹². The selection of a filter resolution is then critical. In Table 1, attenuation reachable with IR filter resolution of 70 and 5 are presented. For the first one, having a monochromatic device is not a limiting factor, compared to telescope defects. For the filter resolution of 5, only a detailed study including aberrations left by the AO system can determine whether or not chromaticity will be dominant.

Parameters	Achievable total nulling (τ)	Theoretical total nulling Strehl = 100% / VLT-like pupil
Step thickness : 0.2 [%]	120668	140 (1300 peak attenuation)
Transition : 1 [μm]	1890 (R = 70, F/D = 48.4)	
Chromaticity (R = 70)	23830	
Chromaticity (R = 5)	121	

Table 1 Manufacturing defects and chromaticity impact on the FQPM efficiency

2.2 Lyot Coronagraphs

A large range of Lyot mask diameters have been manufactured using wet etch lithography process on BK7 glass by Precision Optical Imaging (Rochester, NY, <http://www.precisionopticalimaging.com>). They are made by Cr deposit (+Al) to reach an OD of 6.0 at 1.65 microns. Nine different Lyot masks have been developed with diameter starting from $2.25 \lambda/D$ to $14.40 \lambda/D$.

All these masks were deposited on the same glass substrate ($\lambda/4$) with AR coating on both faces ($R < 1\%$) and allows the selection of a different mask simply by translation along the x and y directions.

In parallel GEPI has produced individuals Lyot masks (4.5, 4.9, $7.5 \lambda/D$) using Cr deposition (+Au) with the same requirements for the OD. In both case accuracy on the mask is close to 1 micron on the diameter and each mask are perfectly circular and clean (see Fig. 3, left). AR coating still needs to be done.

2.3 Apodized Pupil Lyot Coronagraph

General description – We adopt a $4.5 \lambda/D$ APLC configuration based on a previous sensitivity analysis¹³. For this coronagraph, manufacturing of the apodizer is an issue. So far, we explored two techniques : either using a continuous deposit (inconel , for instance) or binary pattern. For the latter, the apodizer is an array of binary pixels, as described hereafter. Since the continuous deposit process has not been successful yet for our application, we will not go into deeper details on that process. However, details related to some devices produced and tested in the context of SPHERE are described in separate papers¹⁴.

Lyot masks – The $4.5 \lambda/D$ hard-edge opaque Lyot mask has been fabricated by GEPI using precise mask pattern of about $1 \mu\text{m}$ accuracy (from Optimask). With the Chrome deposit (20 nm), Au deposit has been added (200 nm) to reach an OD of 6.0 at $1.65 \mu\text{m}$. Antireflection coating still need to be done. A temporary lack of BK7 substrates lead to the use of fused silica substrates with an optical quality of $\lambda/4$ peak-to-valley (ptv).

Microdots apodizer – A binary pixellated apodizer has been designed and fabricated by Precision Optical Imaging using lithography techniques. Such apodizer is an array of pixels that are either blocking or letting through the incident light. It is fabricated by lithography of a light-blocking metal layer deposited on a transparent glass substrate. An error diffusion algorithm was used to optimize the distribution of pixels that best approximates the required field transmission^{15,16,17}. This deterministic algorithm treats the pixels in a lexicographic order (i.e. top to bottom and left to right). It chooses the transmission of a given pixel of the apodizer (either 0 % or 100 %) by comparing the transmission required at this location to a 50 % threshold, i.e. the transmission is set to zero if the required transmission is smaller than 50 %, and to one otherwise. The induced transmission error is “diffused” to adjacent pixels that have not been processed yet by biasing the transmission required at the corresponding locations. This locally cancels the error of the binary optics relative to the required transmission. Such procedure has been used for gray-level reproduction with black-and-white printing techniques¹⁶. Shaping of coherent laser beams has also been demonstrated¹⁷. The error diffusion algorithm is advantageous because the binarization noise is “blue”, i.e. the noise spectral density is only significant at high frequencies. This allows the accurate generation of gray levels and quickly spatially varying shaping functions. In the specific case of the design of a coronagraph, this allows to match the PSF of the binary apodizer to the required apodized PSF within some radial distance (in the control radius of the AO system). In other words, these high frequencies are pushed out of the AO correction domain.

An advantage of a pixellated apodizers versus continuous ones is that the apodizer does not have a spatial phase, while a continuous metal layer with spatially-varying thickness introduces a wavefront error that might compromise cancellation at all radial distances.

In general, better shaping results are obtained as the pixel size decreases¹⁷, since this allows finer control of the local transmission and pushes the binarization noise to higher frequency. In theory, the radial distance under which a good match between the specified PSF and the binary shaper PSF is obtained can be increased by decreasing the pixel size. In practice, the shaping accuracy can be significantly impacted by the actual size and shape of the features of the binary apodizer. Considering the small size of the apodizer (3mm in diameter), it was chosen to use pixels on a 6 microns grid for the binary optics. The mask design was numerically precompensated by estimating the feature size which would be obtained after fabrication¹⁷.

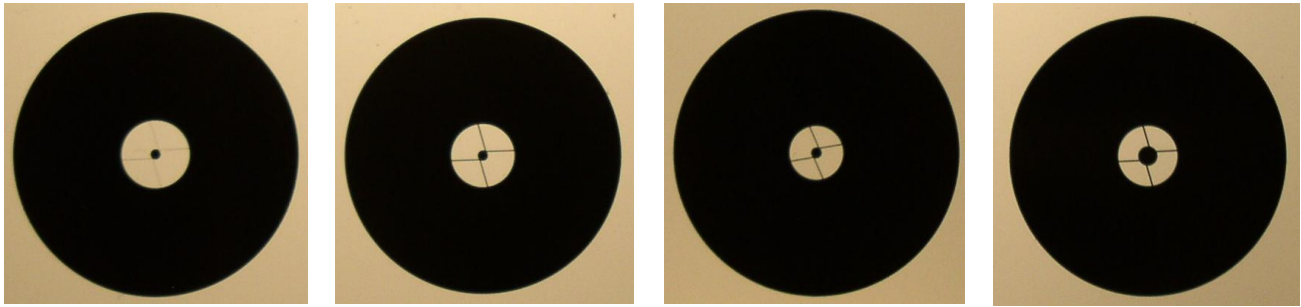


Figure 2 Several high frequencies filters (pupil stop) manufactured with laser-cutting (substrate diameter is 12.7 mm). From left to right : VLT pupil mask (updated), APLC pupil stop, Lyot pupil stop and FQPM pupil stop.

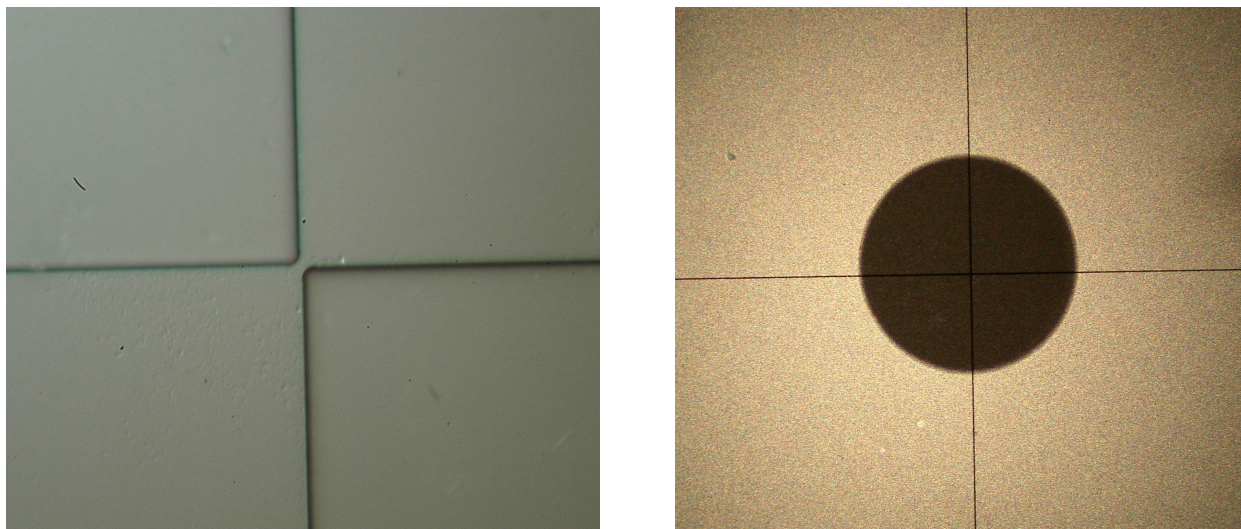


Figure 3 Left : microscopic inspection of the FQPM quadrants (x 50). Peak-to-peak transition is 2 μm and distance between two adjacent transitions is $< 1 \mu\text{m}$. Right : shadowgraph inspection of a 360 μm (diameter) Lyot coronagraph (x 50).

The shaper was fabricated using wet-etch contact lithography of a Cr layer (OD of 4.0) deposited on a glass substrate (BK7, $\lambda/20$). The measured transmission of the apodizer is plotted in Fig. 4, image of the apodizer using a shadowgraph is compared to simulation map as well. The fabricated part matches the field transmission specification within 2.5% (local profile, Fig. 4 bottom left) and 3% (azimuthally average profile, Fig. 4 middle left), and has excellent circular symmetry (Fig. 4, bottom right).

3. LABORATORY RESULTS

Testing our laboratory coronagraphs is relatively recent and still on going. Hence, a comparison of these three devices considered as a baseline for HOT is premature. The intent of these tests on a separate bench was for quality inspection and validation before implementation on HOT. In this section, we will discuss the APLC quality/first results only.

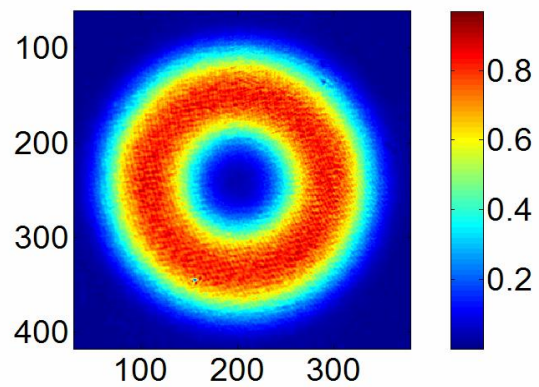
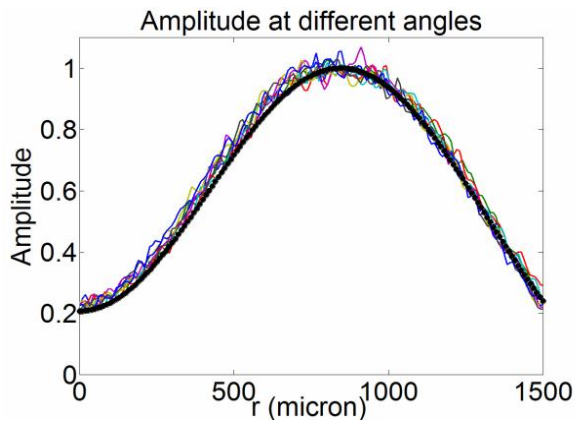
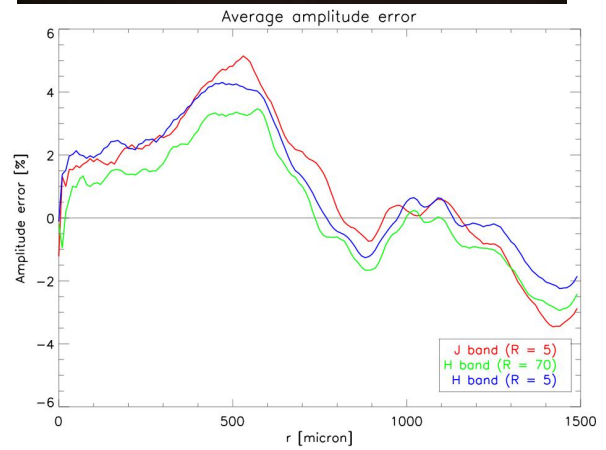
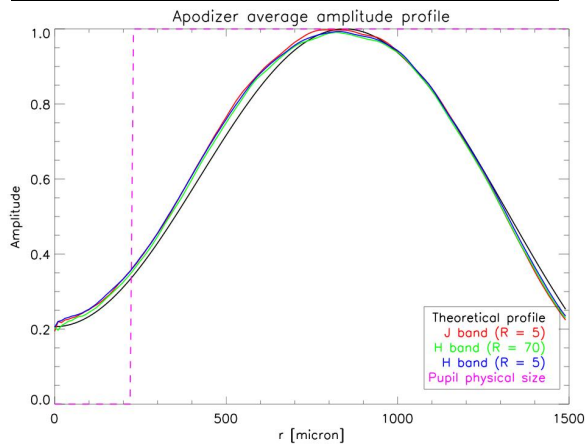
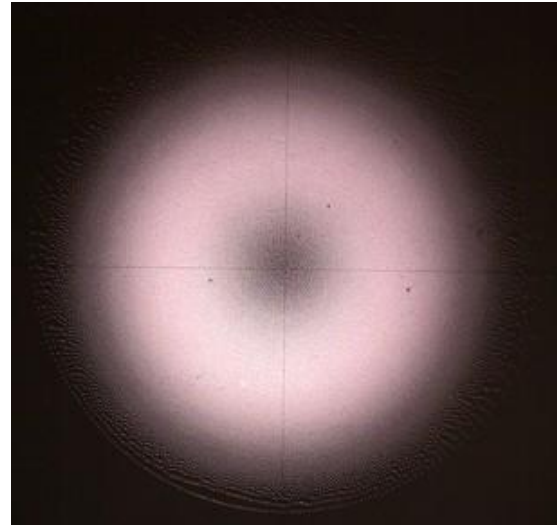
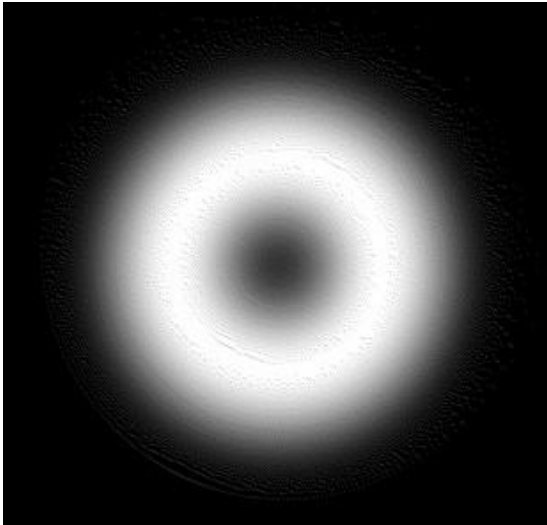


Figure 4 Upper row (left) : Simulation map with 5x5 microns dots, plotted as an example. Upper row (right) : shadowgraph inspection (x20) of the device (real dots are 4.5 x 4.5 microns determined using microscope inspection x100). Middle row (left) : Apodizer azimuthally average profile (from center to the edges) using different filters (J, H and narrow H band) compared to specification. Middle row (right) : corresponding average amplitude error as function of the position using the same filters. Bottom row (left) : profile cut at 8 different angles ($0, \pi/4, \pi/2, \dots, 3\pi/4$), Bottom row (right) : image of the apodizer with IR camera.

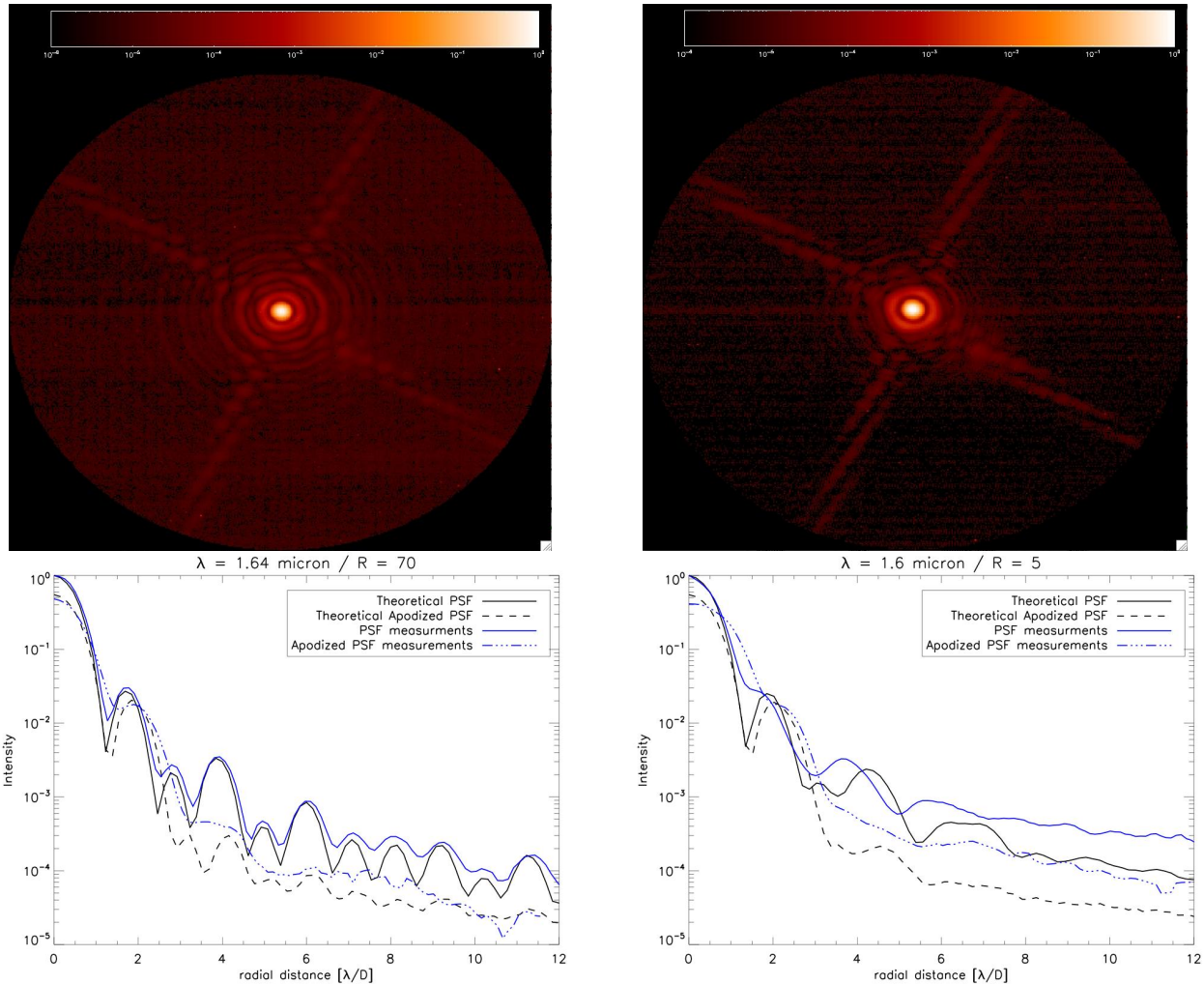


Figure 5 Top row (left) : VLT-like pupil PSF recorded on the bench ($\lambda = 1.64 \mu\text{m}$, $R = 70$). Top row (right) : VLT-like pupil apodized PSF in the same conditions. Bottom (left) : PSF and apodized PSF recorded on the bench (blue lines) compared to theoretical ones (black lines) with narrow H filter ($\lambda = 1.64 \mu\text{m}$, $R = 70$). Bottom (right) : Same measurements as previous ones but with broadband H filter ($R = 5$).

Precise inspection of the quality of the apodizer has been realized in the laboratory (see Fig. 1) where we determined the size of the square chrome dots to $4.5 \times 4.5 \mu\text{m}$ using a microscope. The accuracy on the profile is quite impressive, and is at about 3% of the specifications. Achromaticity of the profile is also demonstrated : error on the profile only increase about 2% from narrow H filter to broadband J filter. The requested accuracy was 5% at $1.64 \mu\text{m}$ indeed. So, even in J band the binary device is in the specifications.

In Fig. 5 we present data recorded on the bench. This first series of tests intends to demonstrate the correct behavior of the binary apodizer on the PSF. In other words, we do not place the Lyot coronagraph on the focal plane but only compare the PSF without apodizer to that with the apodizer. Qualitatively (Fig. 5 top pictures) it is demonstrated that the apodizer works well : the PSF's wings of the apodized PSF has been reduced in intensity and by energy concern one can see that there is more energy inside the core of the apodized PSF compare to the non-apodized one (exposure time are here identical). This behavior agrees well with the theoretical predictions. Apart from some discrepancies between theory and measurements (Fig. 5, bottom, for $R = 5$ in H band), the gain between measured PSF and measured apodized PSF is fully consistent with theory. This results has been demonstrated in H with a narrow filter ($R = 70$) and with a broadband filter as well ($R = 5$).

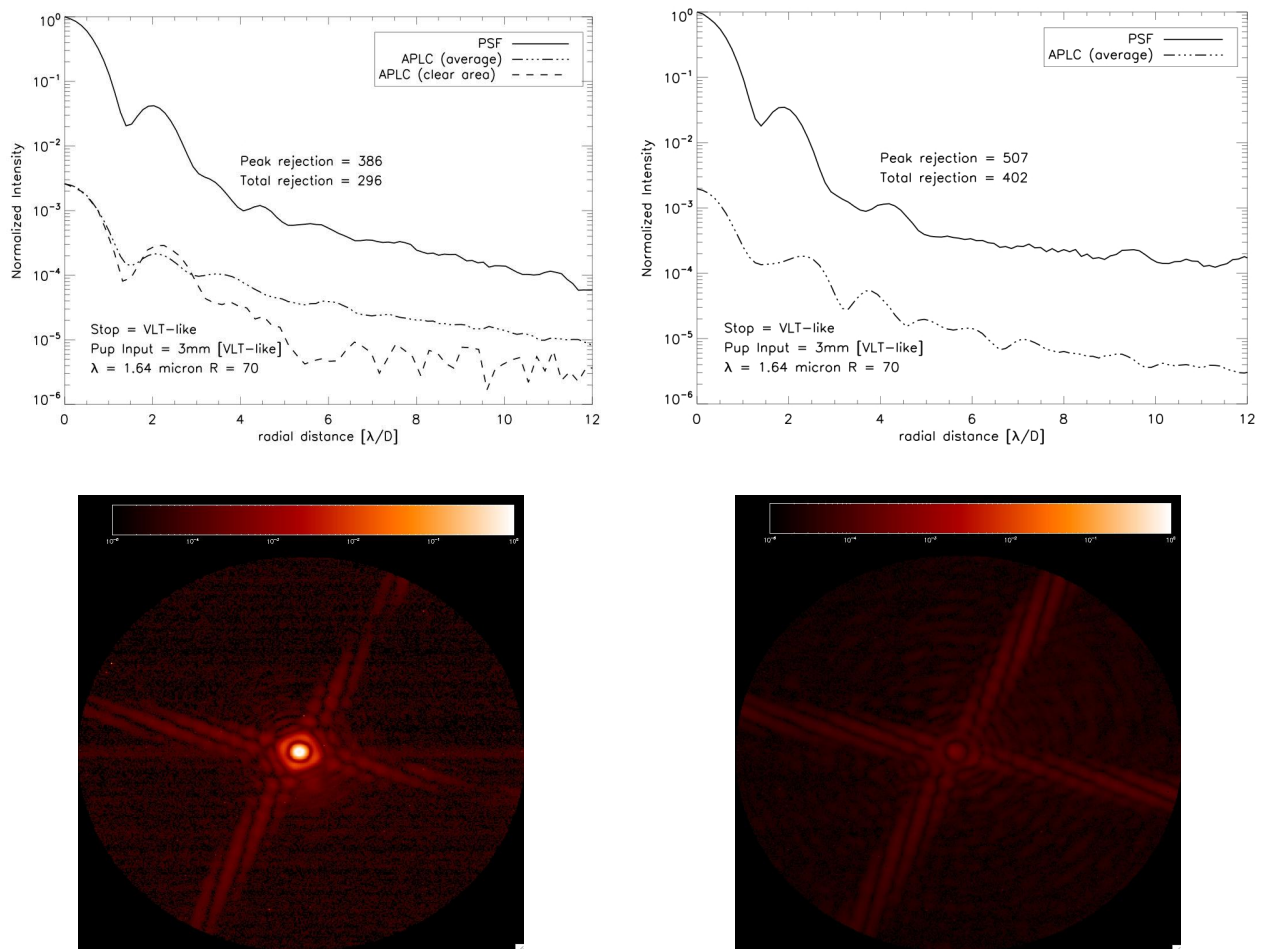


Figure 6 Top left: Results obtained at 1.64 μm ($R = 70$), full line is the apodized PSF, dot line is an azimuthally average of the coronagraphic PSF and dash line is a cut in the clear area between the peak diffraction of the spider vanes on the coronagraphic PSF. Pupil spider vanes are equal on the pupil mask and pupil stop (60 μm). Total rejection is 296 while peak rejection is 386. Top right : first run of test using the updated pupil mask (15 μm spider vanes) : total rejection is 402 and peak rejection is 507. Bottom : images recorded on bench using neutral density for the apodized PSF (left) and without on the coronagraphic PSF (right).

The discrepancy can be well understood since theoretical profile comes from simulation assuming perfect components (pupil mask, apodizer) and ideal propagation through the optical system. The net effect of the binary apodizer on the PSF is then demonstrated and consistent with theory. Its achromaticity in H band is confirmed as well.

The second series of test strives to demonstrate the correct coronagraphic behavior of the whole system (binary apodizer + Lyot focal plane mask). In Fig. 6, results recorded on the bench are presented. As discussed in Sec. 1 our pupil mask has wrong value for the spider vanes thickness (60 μm instead of 15 μm). In the precise case of APLC, the pupil stop has also 60 μm spider vanes thickness. Hence, for this first run of test, alignment of the pupil stop with respect to the pupil mask is an issue and will matters the APLC performance. Alignment is made using a 633 nm laser and tuned at the end on the basis of the final IR image on the detector. Total nulling obtained is 296 and peak attenuation is 386. The discrepancy with theory (total nulling about 1100 and peak attenuation of 1200) can be well understood as misalignment errors in the system. In Fig. 7 (left) we assume in simulation (same condition as on the bench) a pupil shear of 0.4% and 1.2° of mismatch in rotation between the pupil mask and stop (spider orientation issue). The pupil shear refers to the misalignment of the pupil stop with the telescope pupil image (in x- and y-directions) and is express in % of the pupil

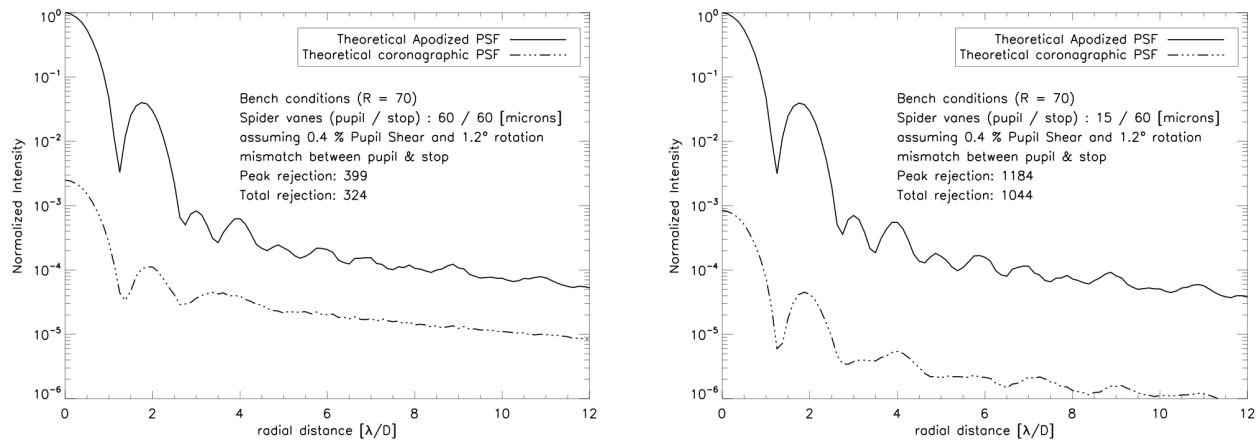


Figure 7 Results from simulation in the bench condition ($R = 70$ H band) assuming 0.4% pupil shear and 1.2° mismatch between pupil and pupil stop. Left : pupil mask and pupil stop with same spider vanes thickness (as used in laboratory, i.e 60 μm). Right : pupil mask updated (spider vanes thickness : 15 μm) in same conditions.

diameter. So, 0.4% pupil shear is equivalent to 12 μm mismatch between the pupil and the stop, hence it is realistic with our experiment conditions. Results derived from simulation are equivalent to that on laboratory.

In Fig. 7 (right) same error conditions are assumed while the entrance pupil spider vanes thickness are updated to the correct value. As a result, performance is consistent with theory since in this case the spider vanes in the pupil stop appear oversized (x4) as expected to avoid any misalignment problem.

First run of test with the updated 15-micron spider vanes pupil mask leads to better performance (Fig. 6, top right) as expected. We are currently implementing a pupil imager system to get rid of misalignment limitations (pupil shear and spider vanes orientation mismatch). Performance will hopefully be improved in the next weeks.

These first tests already confirmed the good behavior of the coronagraphic effect of the APLC using a microdot apodizer.

4. TEST PLAN & FUTUR DEVELOPMENTS

The IR coronagraphic optical path has been installed recently on the High Order Testbench and hence we are currently implementing and testing most of the coronagraph components we developed. Coronagraph devices alignment is an issue and specific solutions for their optimization are currently investigated as pupil imager system for instance. These conditions will enable a realistic comparison between several coronagraphs combined with high order AO correction already started from a theoretical point of view¹⁸. Further investigations on other coronagraph prototyping will be address (such as Band-limited coronagraph¹⁹, for instance).

In the framework of EPICS Phase A, AGPM and Dual Zone prototypes²⁰ will be installed on HOT in 2009/2010. AGPM is currently developed in collaboration between LESIA, IAGL (Institut d'Astrophysique et de Géologie de Liège) and CSL (Centre Spatial de Liège), and is considered for EPICS and SPHERE also (as a possible update of achromatic FPM devices). Dual Zone coronagraph is currently developed by LAM (Laboratoire d'Astrophysique de Marseille) and tested at LESIA in IR for SPHERE.

The High Order Testbench developed at ESO will be an ideal experiment bench for coronagraphy combined with AO. It will take advantage of using two different wavefront sensors such as SHWS and PWS, and make possible comparison between at least 6 different kinds of coronagraph (phase and amplitude-type concepts) in the next years.

5. ACKNOWLEDGEMENTS

The author would thanks Sebastian Tordo and Christophe Dupuis from ESO for helpful support with the ITC and metrology inspection. This activity is supported by the European Community under its Framework Programme 6, ELT Design Study, Contract No. 011863.

REFERENCES

- [1] D. Rouan, P. Riaud, A. Boccaletti, Y. Clénet, and A. Labeyrie. The Four-Quadrant Phase-Mask Coronagraph. I. Principle. *PASP*, 112:1479–1486, November 2000.
- [2] B. Lyot. The study of the solar corona and prominences without eclipses (George Darwin Lecture, 1939). *MNRAS*, 99:580–+, June 1939.
- [3] R. Soummer. Apodized Pupil Lyot Coronagraphs for Arbitrary Telescope Apertures. *ApJ*, 618:L161–L164, January 2005.
- [4] Beuzit, J.-L., Feldt, M., Dohlen, K., et al. 2006a, *The Messenger*, 125, 29
- [5] Macintosh, B., Graham, J., Palmer, D., et al. 2006, in Presented at the Society of Photo-Optical Instrumentation Engineers (SPIE) Conference, Vol. 6272, *Advances in Adaptive Optics II*. Edited by Ellerbroek, Brent L.; Bonaccini Calia, Domenico. Proceedings of the SPIE, Volume 6272, pp. 62720L (2006).
- [6] Kasper, M., Verinaud, C., Beuzit, J.-L., et al. 2007, in *In the Spirit of Bernard Lyot: The Direct Detection of Planets and Circumstellar Disks in the 21st Century*, ed. P. Kalas
- [7] E. Vernet, M. Kasper, C. Vérinaud, E. Fedrigo, S. Tordo, N. Hubin, S. Esposito, E. Pinna, A. Puglisi, A. Tozzi, A. G. Basden, S. J. Goodsell, G. D. Love, and R. M. Myers. Extreme adaptive optics system optimization with the high order test bench. In *Advances in Adaptive Optics II. Edited by Ellerbroek, Brent L.; Bonaccini Calia, Domenico. Proceedings of the SPIE, Volume 6272, pp. 62722K (2006).*, July 2006.
- [8] E. Aller Carpentier, M. Kasper, P. Martinez, E. Vernet, C. Vérinaud, E. Fedrigo, C. Soenke, S. Tordo, N. Hubin, S. Esposito, E. Pinna, A. Puglisi, A. Tozzi, F. Quiros, A. G. Basden, S. J. Goodsell, G. D. Love, R. M. Myers and M. Harrison, High order test bench for extreme adaptive optics system optimization, SPIE 2008
- [9] D. Rouan, A. Boccaletti, P. Baudoz, C. Cavarroc, J. Baudrand, J.M Reess, The Coronagraphic Mode of MIRI/JWST, In the Spirit of Bernard Lyot: The Direct Detection of Planets and Circumstellar Disks in the 21st Century, 2007, ed. P. Kalas
- [10] D. Mawet, P. Riaud, J. Baudrand, P. Baudoz, A. Boccaletti, O. Dupuis, and D. Rouan. The four-quadrant phase-mask coronagraph: white light laboratory results with an achromatic device. *A&A*, 448:801–808, March 2006.
- [11] D. Mawet, P. Riaud, O. Absil, and J. Surdej. Annular Groove Phase Mask Coronagraph. *ApJ*, 633:1191–1200, November 2005.
- [12] P. Riaud, A. Boccaletti, D. Rouan, F. Lemarquis, and A. Labeyrie. The Four-Quadrant Phase-Mask Coronagraph. II. Simulations. *PASP*, 113:1145–1154, September 2001.
- [13] P. Martinez, A. Boccaletti, M. Kasper, P. Baudoz, and C. Cavarroc. Optimization of apodized pupil Lyot coronagraph for ELTs. *A&A*, 474:671–678, November 2007.
- [14] A. Boccaletti, Prototyping achromatic coronagraphs for exoplanet characterization with SPHERE, SPIE 2008
- [15] R. W. Floyd and L. Steinberg, An adaptive algorithm for spatial greyscale, *J. Soc. Inf. Disp.* 17, 7577 (1976).
- [16] R. Ulichney, *Digital Halftoning*, The MIT Press.
- [17] C. Dorrer and J. D. Zuegel, Design and analysis of binary beam shapers using error diffusion, *J. Opt. Soc. Am. B* 24, 1268-1275 (2007)
- [18] P. Martinez et al. Comparison of coronagraphs for high contrast imaging in the context of Extremely Large Telescopes, *A&A* to be submitted 2008.
- [19] M. J. Kuchner and W. A. Traub. A Coronagraph with a Band-limited Mask for Finding Terrestrial Planets. *ApJ*, 570:900–908, May 2002.
- [20]] R. Soummer, K. Dohlen, and C. Aime. Achromatic dual-zone phase mask stellar coronagraph. *A&A*, 403:369–381, May 2003.